Recent Results from the Tevatron Fixed Target and Collider Experiments

Cecilia E. Gerber[a]

[a]Fermi National Accelerator Laboratory
P.O. Box 500, Batavia, IL 60510, USA

We present a review of recent QCD related results from the Fermilab Tevatron fixed target and collider experiments. Topics include jet and boson production, W boson and top quark mass measurements, and studies of CP violation.

1. INTRODUCTION

Quantum Chromodynamics (QCD) emerged as a mathematically consistent theory in the 1970s, and nowadays is regarded as one of the cornerstones of the Standard Model. One of the triumphs of modern particle physics has been the extent to which QCD has successfully accounted for the strong interaction processes observed experimentally at hadron colliders. Some of the processes studied include hadronic jet, heavy quark, and gauge boson production.

The number of new results from the Fermilab Tevatron accelerator that are being presented in over twenty parallel sessions at this conference is overwhelming. The two collider detectors, CDF and DØ, have finished taking data in 1996; new results on Jet and Boson properties are based on these large data sets of ~ 100 pb^{-1} integrated luminosity. Both collaborations are upgrading their detectors in preparation for Run II, scheduled to start in the year 2000. Results from the fixed target experiments are based on data taken during the last fixed target run that ended in 1997. The upcoming fixed target run is scheduled for later this year.

In this summary we review QCD results that are new since last year and that are presented in greater detail in the parallel sessions. We also include the new Tevatron results on the mass of the W boson and the top quark from CDF and DØ. These measurements are used to constrain the mass of the Higgs boson. In addition, we present recent studies of CP violation. The KTeV collaboration has clearly observed direct CP violation in the Kaon system. CDF observes the first indication of CP violation in the b quark system. New results from the NuTeV collaboration are being presented in a different summary contribution to this conference [1].

2. JET PRODUCTION IN PROTON–ANTIPROTON COLLISIONS

At the Tevatron energies, the dominant process in $p\overline{p}$ collisions is jet production. Within the framework of QCD, inelastic scattering between a proton and an antiproton can be described as an elastic collision between a single proton constituent and a single antiproton constituent. These constituents are called partons. After the collision, the outgoing partons manifest themselves as localized streams of particles referred to as “jets”. Theoretical predictions for jet production are given by the folding of the parton scattering cross sections with experimentally determined parton density functions (pdf’s). These predictions have recently improved with next–to–leading order (NLO) QCD scattering calculations [2–4] and new, accurately measured pdf’s [5,6]. Some of the questions that can be addressed with studies of jet production are testing of NLO QCD, extraction of pdf’s, measuring the value of the strong coupling constant α_s, and testing quark compositeness.

2.1. Inclusive Jet Cross Section

The DØ and CDF collaborations measure the central inclusive jet cross section in $p\overline{p}$ collisions at $\sqrt{s} = 1.8$ TeV using an integrated luminosity of 92 pb^{-1} and 87 pb^{-1}, respectively. The inclusive double differential jet cross section can be expressed as:

$$d^2\sigma/(dE_T d\eta) = (N_{Jet})/(\varepsilon \Delta E_T \Delta\eta \int Ldt)$$

where N_{Jet} is the total number of jets observed in a certain jet transverse energy E_T bin, ε is the selection efficiency, ΔE_T is the bin width, $\Delta\eta$ is the pseudorapidity range considered, and $\int Ldt$ is the integrated luminosity associated with the data set. The cross sections are measured in the pseudorapidity interval $0.1 < |\eta| < 0.7$ (CDF, [7]), and the two pseudorapidity ranges $|\eta| < 0.5$ and $0.1 < |\eta| < 0.7$ (DØ, [8]). Fig. 1 shows the ratio plot (Data-Theory)/Theory for the $0.1 < |\eta| < 0.7$ rapidity range for CDF and DØ data compared to NLO QCD.

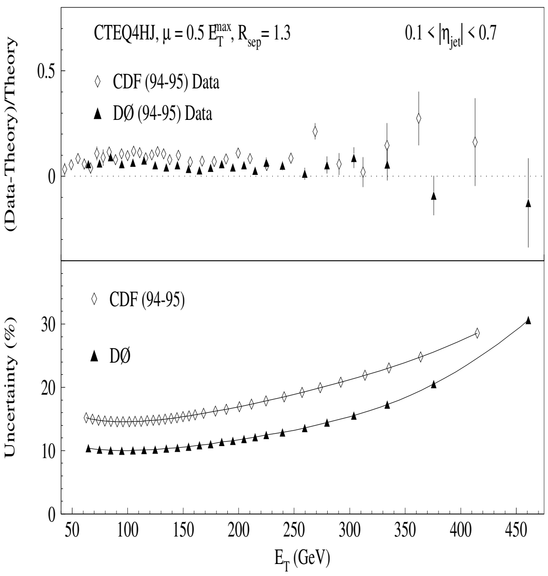

Figure 1. Inclusive jet cross section in the central rapidity region for CDF and DØ, plotted versus jet E_T. The data points are shown with statistical uncertainties. The systematic uncertainty on the ratio is shown in the bottom half of the plot.

In addition, DØ presented for the first time the preliminary [9] measurement of the rapidity dependence of the inclusive jet cross section, which extends the measurement to two forward rapidity regions: $0.5 < |\eta| < 1.0$ and $1.0 < |\eta| < 1.5$. Fig. 2 shows the ratio plot (Data-Theory)/Theory for this measurement. All the measurements show good agreement with the NLO QCD predictions currently available.

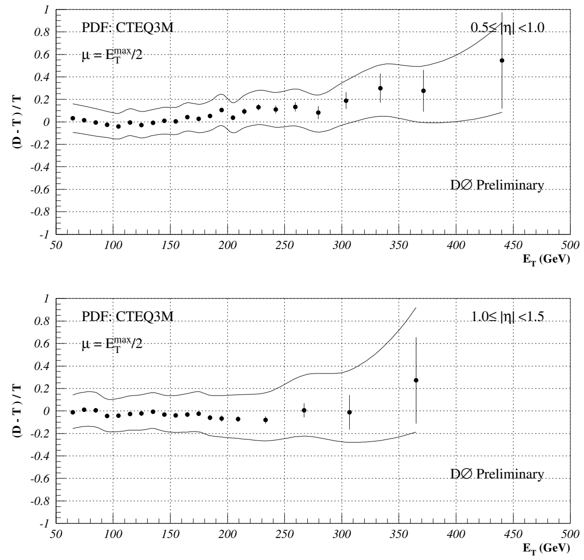

Figure 2. Rapidity dependence of the inclusive jet cross section plotted versus jet E_T from DØ. The systematic uncertainty on the ratio is shown as a band.

Although the Tevatron nominally operated at a center of mass energy of 1.8 TeV, a short period of the time was devoted to collect data at the lower center of mass energy of $\sqrt{s} = 630$ GeV. DØ [9] and CDF [7] measure the ratio of scale invariant cross section $\sigma_S = (E_T^3/2\pi)(d^2\sigma/dE_T d\eta)$ at two

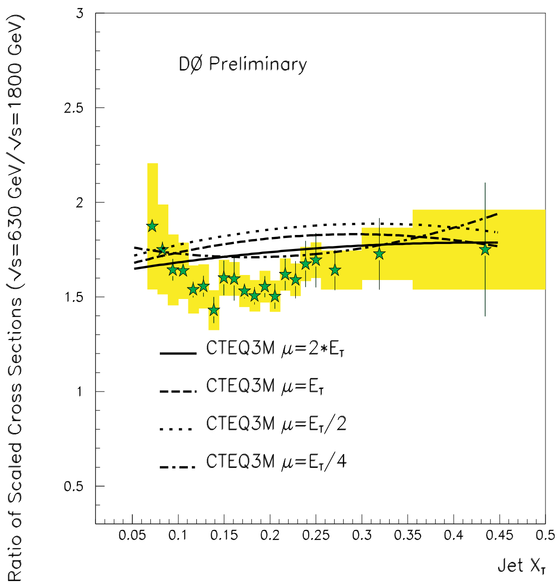

Figure 3. Scale invariant cross section from DØ. Data points are shown with statistical uncertainty; systematic uncertainty is shown as a band. The NLO QCD theoretical predictions for different renormalization scales are shown as lines.

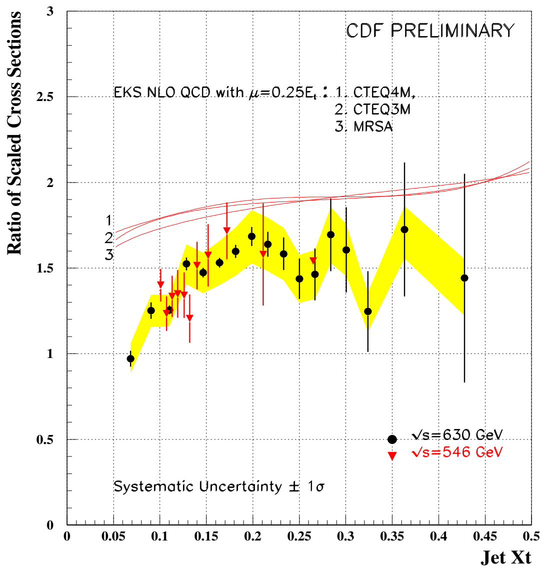

Figure 4. Scale invariant cross section from CDF. Data points are shown with statistical uncertainty; systematic uncertainty is shown as a band. The NLO QCD theoretical predictions for different renormalization scales are shown as lines.

center of mass energies as a function of Jet $x_T = E_T/(\frac{\sqrt{s}}{2})$. Figs. 3 and 4 show the preliminary results for DØ and CDF respectively. NLO QCD overestimates the DØ data by almost three standard deviations in the medium range of x_T. The disagreement between data and theory is even worse for the CDF data at low x_T. A good quantitative agreement between DØ data and NLO QCD can be obtained if different renormalization scales are used in the theoretical calculation at the two different center–of–mass energies. For instance, a scale of $\mu = 2E_T$ at $\sqrt{s} = 630$ GeV and of $\mu = E_T/2$ at $\sqrt{s} = 1800$ GeV reproduces the DØ data best.

CDF [7] extracts the value of the strong coupling constant α_s in the jet E_T range from 40 – 250 GeV by comparing the measured inclusive jet cross section to the NLO JETRAD [10] Monte Carlo. The evolution of the coupling constant over a wide range of scales is clearly observed and is in agreement with QCD predictions. The measured $\alpha_s(E_T)$ is evolved to $\alpha_s(M_Z)$ using a two–loop renormalization group equation. The preliminary measurement is $\alpha_s(M_Z) = 0.1129 \pm 0.0001(\text{stat})^{+0.0078}_{-0.0089}(\text{exp syst})$.

2.2. Dijet Production

CDF and DØ measure the jet production cross section for events with two jets as a function of the dijet invariant mass. The results are shown in figure 5. NLO QCD is in good agreement with the data. DØ's measurement of the dijet mass spectrum [11] is used to search for quark compositeness, which would manifest itself as an excess of events at high masses. A mass scale Λ characterizes both the strength of the quark substructure binding and the physical size of the composite state. Limits are set assuming that

$\Lambda \gg \sqrt{s}$ such that quarks appear to be point-like and the coupling can be approximated by a four–Fermion contact interaction. The best sensitivity is obtained by taking the ratio of the dijet cross sections for events in which both jets are central ($|\eta| < 0.5$) and events in which both jets are forward ($0.5 < |\eta| < 1.0$). The 95% confidence level lower limits on the mass scale are $\Lambda^+ = 2.7$ TeV and $\Lambda^- = 2.4$ TeV for destructive and constructive interference models respectively.

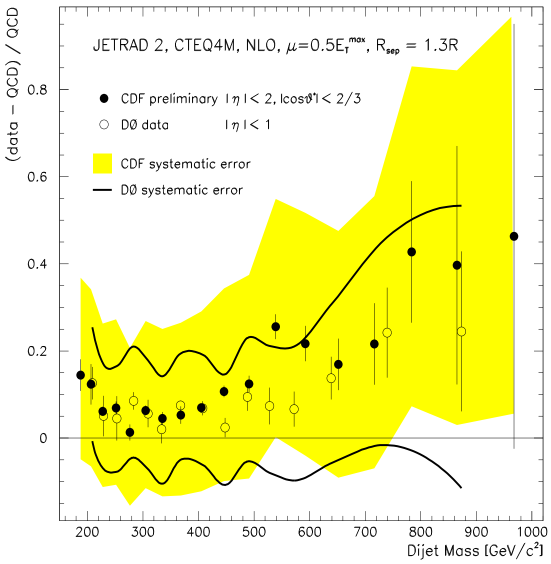

Figure 5. Dijet cross section as a function of the dijet invariant mass from CDF and DØ. Data are compared to NLO QCD with CTEQ4M parton density function.

CDF measures the inclusive dijet differential cross section [12] $d^3\sigma/(dE_1^T d\eta_1 d\eta_2)$ as a function of the trigger jet E_1^T. The trigger jet is central ($0.1 < |\eta| < 0.7$); the second jet pseudorapidity is in one of the following four bins: $0.1 < |\eta| < 0.7$, $0.7 < |\eta| < 1.4$, $1.4 < |\eta| < 2.1$, $2.1 < |\eta| < 3.0$. The four resulting cross sections are shown in figure 6. The measurement is sensitive to the choice of pdf, and CTEQ4HJ qualitatively reproduces CDF data best.

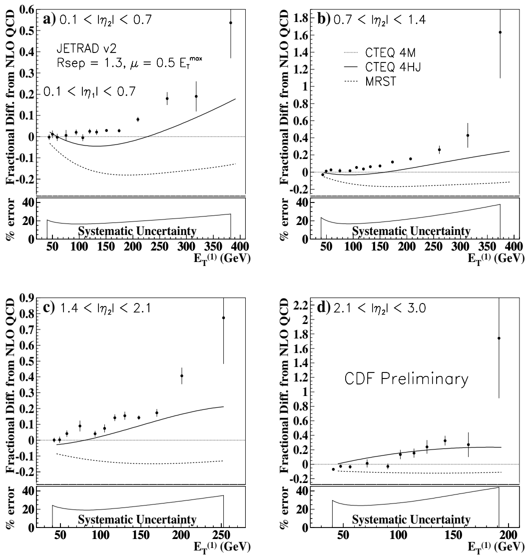

Figure 6. Inclusive Dijet differential cross section as a function of the leading central jet E_T from CDF. Data are compared to the prediction by JETRAD using different parton density functions.

The DØ calorimeter allows the measurement of the energies of jets in the very forward rapidity region permitting a determination of the inclusive dijet differential cross section [13] as a function of the leading and next–to–leading jet E_T in four pseudorapidity bins: $|\eta| < 0.5$, $0.5 < |\eta| < 1.0$, $1.0 < |\eta| < 1.5$, $1.5 < |\eta| < 2.5$. Two topologies are considered: $\eta_1 = \eta_2$ ("same side") and $\eta_1 = -\eta_2$ ("opposite side"), with both jets required to be in the same $|\eta|$ bin. The eight resulting cross sections are shown in figures 7 and 8. The measurement is sensitive to the choice of pdf and CTEQ4M qualitatively reproduces the DØ data well.

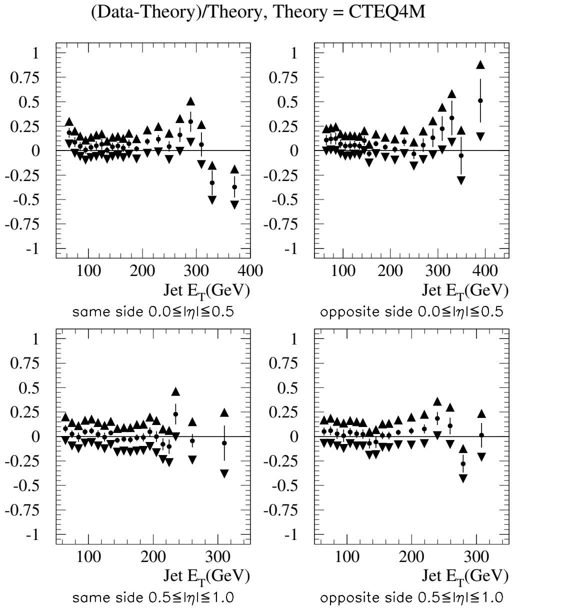

Figure 7. Inclusive Dijet Differential cross section from DØ for "same side"(left) and "opposite side"(right) jet topologies. Data are compared to NLO QCD with the CTEQ4M parton density function.

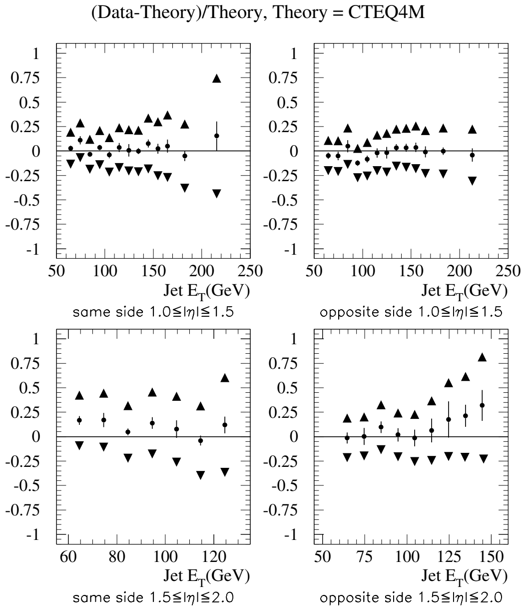

Figure 8. Inclusive Dijet Differential cross section from DØ, for "same side"(left) and "opposite side"(right) jet topologies. Data are compared to NLO QCD with the CTEQ4M parton density function.

2.3. Subjet Multiplicity in Quark and Gluon Jets

DØ measures the subjet multiplicity in jets reconstructed using the k_T algorithm [14]. Jets with $55 < E_T < 100$ GeV and $|\eta| < 0.5$ are selected from data taken at two center–of–mass energies, $\sqrt{s} = 1800$ GeV and $\sqrt{s} = 630$ GeV.

HERWIG [15] predicts that 59% (33%) of the jets are gluon jets at $\sqrt{s} = 1800$ GeV ($\sqrt{s} = 630$ GeV); this information is used to extract the average subjet multiplicity in gluon ($< N_G >$) and quark ($< N_Q >$) jets. DØ clearly distinguishes, on a statistical bases, between quark and gluon jets, as can be seen in figure 9. The measured value of $R \equiv (< N_G > -1)/(< N_Q > -1) = 1.91 \pm 0.04(\mathrm{stat}))^{+0.23}_{-0.19}(\mathrm{syst})$ agrees with the Monte Carlo prediction of $R = 1.86 \pm 0.08(\mathrm{stat})$.

2.4. Diffractive Jet Production

DØ observes the production of dijet events produced in conjunction with two forward rapidity gaps (no calorimeter or scintillator hits in $3.0 < |\eta| < 5.2$) along the directions of each of the initial beam particles in proton–antiproton collisions at the center of mass energies of $\sqrt{s} = 1800$ GeV and $\sqrt{s} = 630$ GeV [16]. This topology is consistent with Hard Double Pomeron exchange. It is interesting to examine the E_T spectrum of the jets produced in these diffractive events. Fig. 10 shows the E_T spectra of the two leading jets for an inclusive sample with two central jets greater than 15 GeV (solid histogram), a sample with the additional requirement of a single forward rapidity gap (dashed histogram) and a sample of double gap events (open circles). All three spectra are in good agreement where the data are available, im-

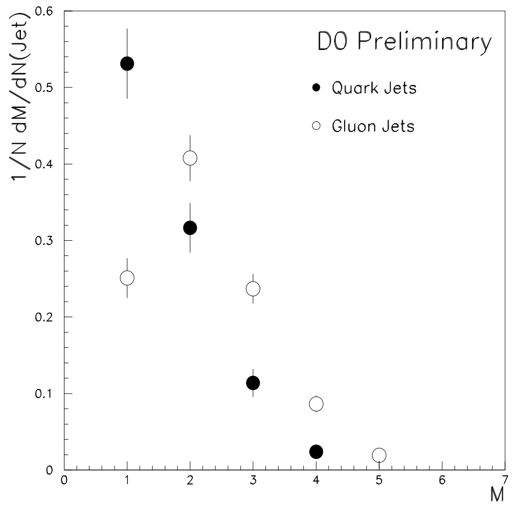

Figure 9. Subjet multiplicity for quark and gluon jets as measured by DØ.

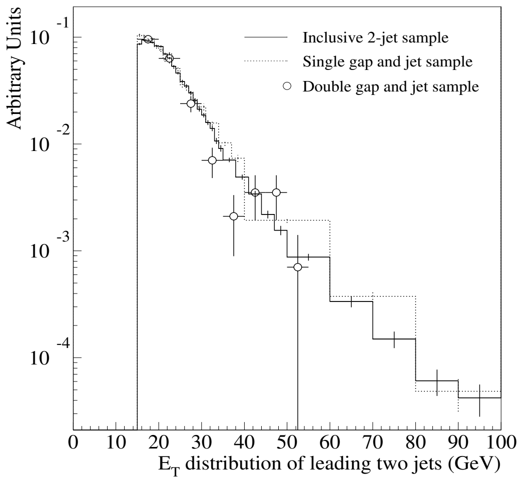

Figure 10. E_T distributions of the leading two jets for three data samples at $\sqrt{s}$ = 1800 GeV from DØ: inclusive dijet sample (solid histogram), sample with one forward rapidity gap (dotted line) and double gap events (circles).

plying that the dynamics of leading jets produced in the rapidity gap events appear to be similar to those of inclusive QCD production. The same behavior is observed in data taken at the lower center of mass energy of $\sqrt{s}$ = 630 GeV. The E_T spectra at both center of mass energies looks harder than allowed by the 5% rule–of–thumb for the pomeron momentum fraction.

CDF observes diffractive dijet production associated with a leading antiproton in $p\overline{p}$ collisions at $\sqrt{s} = 630$ GeV in data taken with the roman–pot trigger [17]. Using the diffractive dijet events in the kinematic region of the momentum loss fraction of the antiproton $0.04 < \xi < 0.10$ and the four momentum transfer squared $|t| < 0.2$ GeV^2, CDF finds that the cross section ratio of diffractive to non-diffractive dijet events as a function of the momentum fraction of the parton in the antiproton participating in the dijet production $x_{\overline{p}}$ decreases with increasing $x_{\overline{p}}$, as can be seen in figure 11. Similar results are observed in data taken at the center of mass energy of $\sqrt{s} = 1800$ GeV.

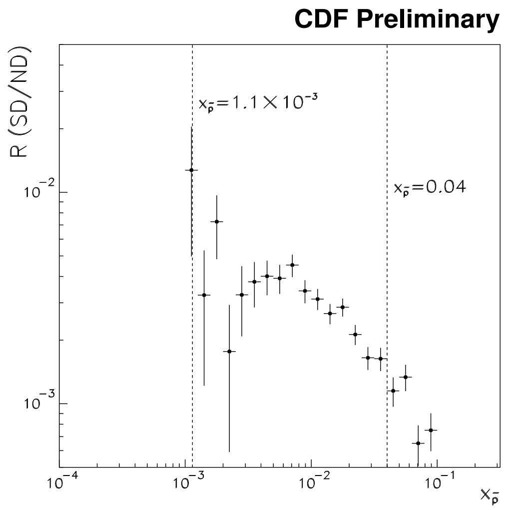

Figure 11. Ratio of single diffractive to non–diffractive dijet events as a function of $x_{\overline{p}}$ at $\sqrt{s} = 630$ GeV from CDF.

3. BOSON PRODUCTION

W and Z bosons, the carriers of the weak force, are directly produced in high energy $p\overline{p}$ collisions at the Fermilab Tevatron. In addition to probing electroweak physics, the study of the production of W and Z bosons provides an avenue to explore QCD, the theory of strong interactions. Direct production of photons is also a powerful tool for testing QCD predictions with fewer of the ambiguities associated with jet production and fragmentation. The measurement of the high mass Drell–Yan cross section above the Z mass tests for quark–lepton compositeness.

3.1. W and Z Production in $p\overline{p}$ collisions

Large numbers of W bosons have been detected by the two collider detectors (CDF and DØ) during the 1992–1996 running period. These samples complement the detailed studies carried out on the Z boson at LEP and SLC, and also the new W studies from LEP II.

DØ measures the production cross section times branching ratio for W and Z bosons. The product of the W boson cross section and the branching fraction for $W \to e\nu$ is calculated using the relation

$$\sigma(p\overline{p} \to W + X) \cdot B(W \to e\nu) = \frac{N^W_{obs}\left(1 - f^W_{QCD}\right) - \epsilon_W N^Z_{obs}(1 - f^Z_{QCD})\frac{A^W_{Z_{ee}} + A^W_{Z_\tau}}{A_Z \epsilon_Z}}{\epsilon_W A_W \left(1 + \frac{A^W_{W_\tau}}{A_W}\right) \mathcal{L}}$$

where N^W_{obs} and N^Z_{obs} are the number of $W \to e\nu$ and $Z \to ee$ candidate events; f^W_{QCD} and f^Z_{QCD} are the fraction of the $W \to e\nu$ and $Z \to ee$ candidate events that come from multijet, b quark, and direct photon background sources; ϵ_W and ϵ_Z are the efficiency for $W \to e\nu$ and $Z \to ee$ events to pass the selection requirements; A_W and A_Z are the geometric and kinematic acceptance for $W \to e\nu$ and $Z \to ee$ which include effects from detector resolution; $A^W_{W_\tau}$, $A^W_{Z_{ee}}$ and $A^W_{Z_\tau}$ are the fraction of $W \to \tau\nu$ $Z \to ee$ and $Z \to \tau\tau$ events that passes the $W \to e\nu$ selection criteria; and $\mathcal{L}$ is the integrated luminosity of the data sample.

The product of the Z boson cross section and the branching fraction for $Z \to ee$ is determined from the relation

$$\sigma(p\overline{p} \to Z + X) \cdot B(Z \to ee) = \frac{N^Z_{obs}\left(1 - f^Z_{QCD}\right)\left(1 - f_{DY}\right)}{\epsilon_Z A_Z \mathcal{L}}$$

where f_{DY} is a correction for the Drell-Yan contribution to Z boson production. The results are summarized in table 1.

The ratio of the cross sections can be used to extract an indirect measurement of the total width of the W boson. In the ratio, many of the systematic uncertainties, including the luminosity uncertainty, cancel. This method therefore gives the most precise determination of the W width currently available. The result on the cross section ratio is summarized in table 1. Using this results we can determine the electronic branching fraction of the W boson via $B(W \to e\nu) = \mathcal{R}B(Z \to ee)\frac{\sigma_Z}{\sigma_W}$. Using $B(Z \to ee) = 0.03367 \pm 0.00006$ [18] and $\sigma_W/\sigma_Z = 3.29 \pm 0.03$ [19], we get $B(W \to e\nu) = 0.1066 \pm 0.0015$ (stat) $\pm\ 0.0021$ (syst) $\pm\ 0.0011$ (other) $\pm\ 0.0011$ (NLO), where the next-to-last source of uncertainty comes from uncertainties in $B(Z \to ee)$ and in σ_W/σ_Z. Assuming the standard model prediction for the electronic partial width (0.2270 ± 0.0011 GeV [20]), we can calculate the W boson width $\Gamma_W = \Gamma^e_W/B(W \to e\nu)$ as $\Gamma_W \pm 0.030$ (stat) $\pm\ 0.041$ (syst) $\pm\ 0.022$ (other) $\pm\ 0.021$ (NLO) GeV, to be compared with the standard model prediction of $\Gamma_W = 2.094$ ± 0.006 GeV [20]. The difference between our measured value and the standard model prediction, which is the width for the W boson to decay to final states other than the two lightest quark doublets and the three lepton doublets, is thus 0.036 ± 0.060 GeV. This is consistent with zero within uncertainties, so we set a 95% confidence level upper limit on the W boson width to non-standard-model final states ("invisible width") of 0.168 GeV.

CDF and DØ measure the differential $d\sigma/dp_T$ distribution for W and Z bosons decaying to electrons. The data agrees with the combined QCD perturbative and resummation calculations [21, 22], as can be seen in figure 12 for the DØ W data, and in figure 13 for the CDF Z data. In addition, the $d\sigma/dp_T$ distribution for the Z boson discriminates between different vector boson production models and can be used to extract values of the non-perturbative parameters for the resummed prediction from a fit to the differential cross section. Fig. 14 compares DØ Z data to the fixed-order perturbative QCD theory [23] in terms of a percentage difference from the prediction. We observe a strong disagreement at low-p_T, as expected due to the divergence of the NLO calculation at $p_T = 0$, and a significant enhancement of the cross section relative to the prediction at moderate values of p_T, confirming the enhancement of the cross section from soft gluon emission.

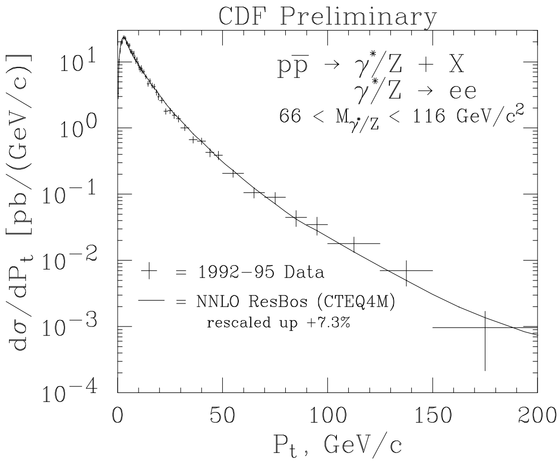

Figure 13. The Z boson transverse momentum spectrum, showing the CDF result (solid points) with total uncertainty. The data have been unfolded for detector resolutions and are compared to the theoretical calculation by Balasz and Yuan [22], scaled up 7.3% to match the measured inclusive Z production cross section.

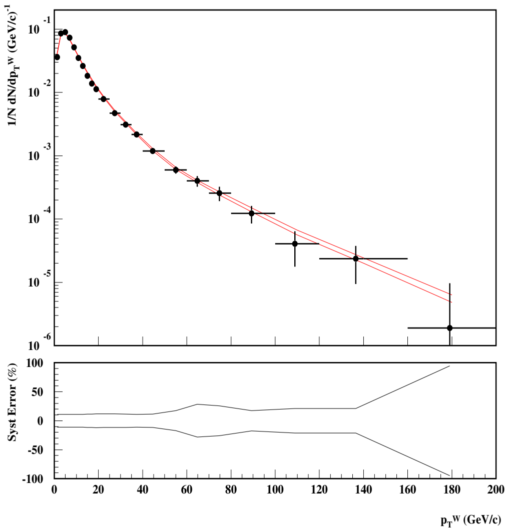

Figure 12. The W boson transverse momentum spectrum, showing the DØ result (solid points) with statistical uncertainty. The theoretical calculation by Arnold and Kauffman [21], smeared for detector resolutions, is shown as two lines corresponding to the $\pm 1\sigma$ variations of the uncertainties in the detector modeling. The fractional systematic uncertainty on the data is shown as a band in the lower portion of the plot.

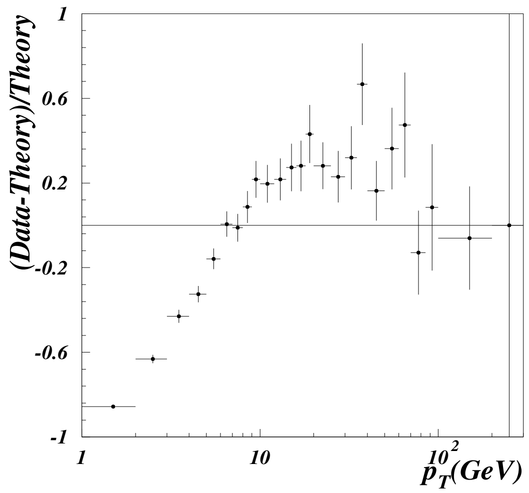

Figure 14. Fractional difference between DØ Z transverse momentum data and the fixed-order calculation from Arnold and Reno [23].

Table 1
The DØ preliminary cross sections for W and Z bosons and their ratio.

	Value	Uncertainty Contribution (pb)
N^W_{obs}	67078	10
ϵ_W	0.671 ± 0.009	30
A_W	0.465 ± 0.004	20
f^W_{QCD}	0.064 ± 0.014	35
$(A^W_{Zee} + A^W_{Z\tau})/A_Z$	0.133 ± 0.034	–
ϵ_Z	0.744 ± 0.011	–
f^Z_{QCD}	0.045 ± 0.005	–
N^W_Z	621 ± 155	6
$A^W_{W\tau}/A_W$	0.0211 ± 0.0021	5
$\mathcal{L}$	84.5 ± 3.6 pb^{-1}	100
$\sigma(p\overline{p} \to W + X) \cdot B(W \to e\nu)$	2310 ± 10(stat) $\pm$ 50(syst) $\pm$ 100(lum) pb	
N^Z_{obs}	5397	3
ϵ_Z	0.744 ± 0.011	3
A_Z	0.366 ± 0.003	2
f^Z_{QCD}	0.045 ± 0.005	1
f_{DY}	0.012 ± 0.001	< 1
$\mathcal{L}$	84.5 ± 3.6 pb^{-1}	10
$\sigma(p\overline{p} \to Z + X) \cdot B(Z \to ee)$	221 ± 3(stat) $\pm$ 4(syst) $\pm$ 10(lum) pb	
N^W_{obs}/N^Z_{obs}	12.43 ± 0.18	0.15
ϵ_Z/ϵ_W	1.108 ± 0.007	0.06
A_Z/A_W	0.787 ± 0.007	0.09
$(A^W_{Zee} + A^W_{Z\tau})/A_Z$	0.133 ± 0.034	0.03
f^W_{QCD}	0.064 ± 0.014	0.16
f^Z_{QCD}	0.045 ± 0.005	0.05
f_{DY}	0.012 ± 0.001	0.01
$A^W_{W\tau}/A_W$	0.021 ± 0.002	0.02
$\mathcal{R}$	10.43 ± 0.15(stat) $\pm$ 0.20(syst) $\pm$ 0.10(NLO)	

3.2. Photon Production

CDF measures the inclusive photon cross section [24] in the central region $|\eta| < 0.9$ using 87 pb^{-1} taken during the 1994–1995 $p\overline{p}$ collider run. Fig. 15 shows the data compared to variations of the model by Vogelsang *et al.*[25], in which the renormalization, fragmentation and factorization scales are changed independently. None of these changes allows the theory to agree with the data over the entire E_T region.

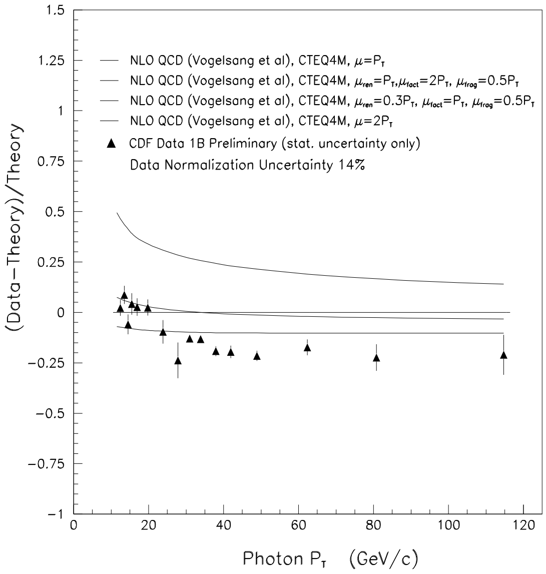

Figure 15. Comparison of the CDF inclusive photon cross section with the latest QCD predictions [20] shown using a wide range of scale choices.

CDF also measures the production of a photon plus a muon [24] and probes the charm content of the proton via the reaction $cg \rightarrow c\gamma \rightarrow \gamma\mu X$. Results for the production cross section are compared with a NLO calculation and to PYTHIA [26] Monte Carlo. The latter, which does not include bremsstrahlung radiation, falls below the data; the data are consistent with the NLO prediction.

E706 [27] uses data accumulated from a proton beam at 800 GeV/c on Be target and measures the π^0 and direct–photon inclusive cross section as functions of p_T. The measurements are shown in figure 16 compared to NLO QCD with and without k_T enhancement [28]. Current pQCD calculations fail to account for the measured cross sections using conventional choices of scales. A simple implementation of supplemental parton k_T in pQCD calculations [29], with $< k_T >\sim 1$, provides a reasonable description of the data. E706 obtained similar results using a proton beam at 530 GeV/c, and a π^- beam at 515 GeV/c, and using a hydrogen target.

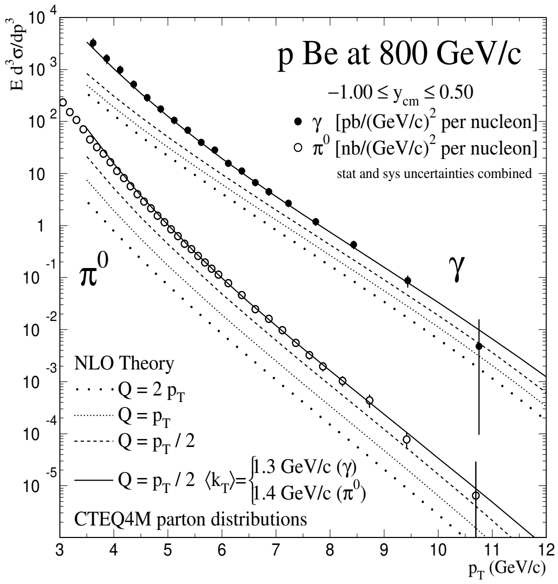

Figure 16. Invariant cross sections for direct–γ and π^0 production from E706. Curves represent the NLO pQCD prediction with and without supplemental parton k_T smearing.

3.3. Drell–Yan production

E866 measures the Drell–Yan cross sections to muon pairs [31] with dimuon mass $M_{\mu^+\mu^-} \geq$ 4.5 GeV/c from an 800 GeV/c proton beam incident on hydrogen and deuterium targets. The ratio of $\overline{d}/\overline{u}$ in the proton as a function of Bjorken x is determined from the ratio of Drell–Yan cross sections. The result is shown in figure 17. The ratio $\overline{d}/\overline{u}$ decreases with x for $x > 0.2$. However, at moderate x, $0.05 < x < 0.2$, it clearly is different from one and only approaches unity as $x \to 0.025$.

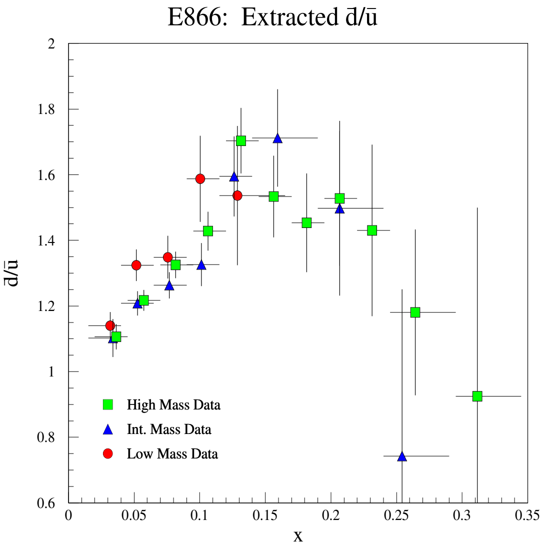

Figure 17. The ratio $\overline{d}/\overline{u}$ in the proton as a function of x extracted from the E866 cross section ratios.

DØ measures the Drell–Yan cross section in the dielectron invariant mass range from 50 to 1000 GeV$/c^2$ using 120 pb^{-1} of data collected in $p\overline{p}$ collisions at $\sqrt{s} = 1.8$ TeV. No deviation from the standard model expectations is observed, and the data are used to set limits on the energy scale of quark–electron compositeness with common constituents. The 95% confidence level lower limits on the compositeness scale vary between 3.3 TeV and 6.1 TeV depending on the assumed form of the effective contact interaction [30].

4. MEASUREMENT OF THE W MASS

In the standard model of the electroweak interactions, the mass of the W boson is predicted to be

$$m_W = \left(\frac{\pi\alpha(m_Z{}^2)}{\sqrt{2}G_F}\right)^{\frac{1}{2}} \frac{1}{\sin\theta_w\sqrt{1-\Delta r_W}} \, . \qquad (1)$$

In the "on-shell" scheme [35] $\cos\theta_w = m_W/m_Z$, where m_Z is the Z boson mass. A measurement of m_W, together with m_Z, the Fermi constant (G_F), and the electromagnetic coupling constant (α), determines the electroweak radiative corrections Δr_W experimentally. Purely electromagnetic corrections are absorbed into the value of α by evaluating it at $Q^2 = m_Z{}^2$ [36]. The dominant contributions to Δr_W arise from loop diagrams that involve the top quark and the Higgs boson. The correction from the $t\overline{b}$ loop is substantial because of the large mass difference between the two quarks. It is proportional to m_t^2 for large values of the top quark mass m_t. Since m_t has been measured at the Tevatron, this contribution can be calculated within the Standard Model. For a large Higgs boson mass, m_H, the correction from the Higgs loop is proportional to $\ln m_H$. If additional particles which couple to the W boson exist, they would give rise to additional contributions to Δr_W. Therefore, a measurement of m_W is one of the most stringent experimental tests of SM predictions. Deviations from the predictions may indicate the existence of new physics. Within the SM, measurements of m_W and the mass of the top quark constrain the mass of the Higgs boson. A discrepancy with the range allowed by the Standard Model could indicate new physics. The experimental challenge is thus to measure the W boson mass to sufficient precision, about 0.1%, to be sensitive to these corrections.

CDF and DØ report precise new measurements of the W boson mass based on an integrated luminosity of $\sim$ 100 pb^{-1} from $p\overline{p}$ collisions at $\sqrt{s} = 1.8$ TeV. CDF identifies W bosons by their decays to $e\nu$ and $\mu\nu$, with electrons and muons identified in the central pseudorapidity region of the detector. The combined CDF result [37] for m_W is $m_W(\mathrm{CDF}) = 80.433 \pm 0.079$ GeV. DØ identifies W bosons by their decays to $e\nu$, with electrons identified both in the central and the forward pseudorapidity region. The combined DØ result [38] for m_W is $m_W(\mathrm{D\O}) = 80.474 \pm 0.093$ GeV. The Tevatron values are combined

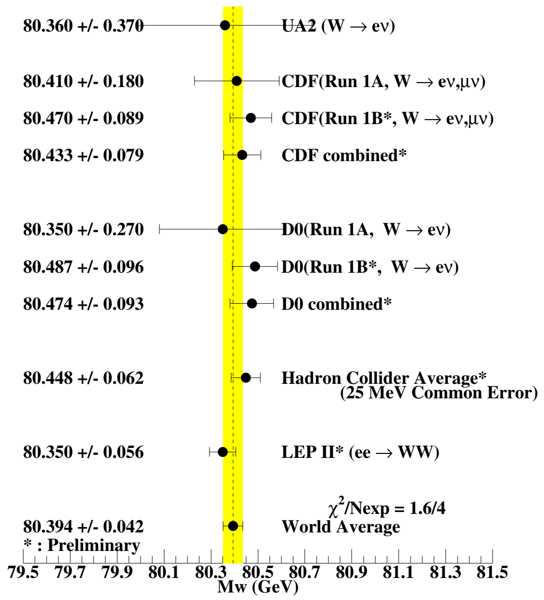

Figure 18. Summary of current direct measurements of the W mass. The world average is shown as the band.

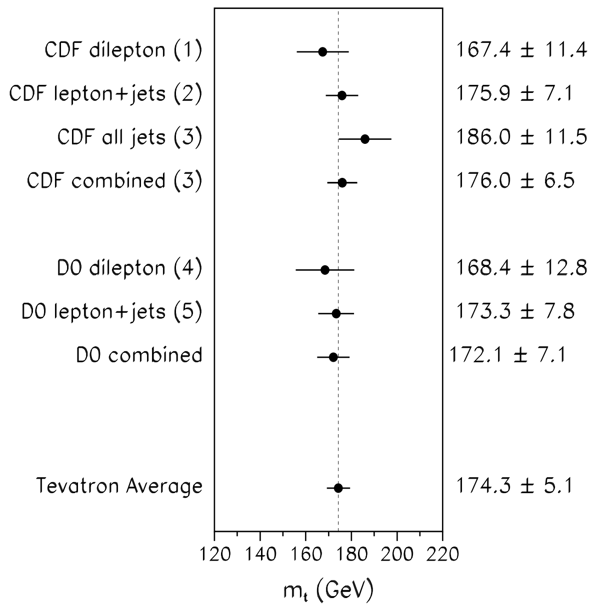

Figure 19. Summary of current measurements of the top quark mass from the Fermilab collider experiments CDF and DØ. The combined result is shown as a line.

with a 25 MeV common error, covering common uncertainties in pdf's, W width and QED corrections to give: $m_W(\text{Tevatron}) = 80.450 \pm 0.063$ GeV. The inclusion of the UA2 data produces a hadron collider average of $m_W(\overline{p}p) = 80.448 \pm 0.062$ GeV. Including LEP2 gives a world average of direct W mass measurements of $m_W(\text{direct}) = 80.410 \pm 0.044$ GeV. The various measurements can be seen in figure 18. Fig. 19 shows the current results for the top quark mass measurements from CDF and DØ. Fig. 20 compares the direct measurements of the W boson and top quark masses to the values predicted by the Standard Model for a range of Higgs mass values [39].The measured values are in agreement with the prediction of the Standard Model.

5. STUDIES OF CP VIOLATION

CDF reports an updated [32] direct measurement of the Standard Model CP violation parameter sin2β using 110 pb^{-1} of data collected in $p\overline{p}$ collisions at $\sqrt{s} = 1.8$ TeV. CP violation can manifest itself as an asymmetry in the decay rate of particle versus antiparticle to a particular final state:

$$A_{CP} = \frac{N(\overline{B^0} \to J/\psi K_S^0) - N(B^0 \to J/\psi K_S^0)}{N(\overline{B^0} \to J/\psi K_S^0) + N(B^0 \to J/\psi K_S^0)}.$$

In the Standard Model, this CP asymmetry is proportional to sin2β. A value of sin2$\beta > 0$ would indicate CP violation in the b quark system.

CDF uses a signal sample that consists of 400 $B \to J/\psi K_S^0$ events. About half of the events have both muon tracks fully contained within the silicon vertex detector, and therefore have precision lifetime information. Three tagging methods are used to identify the flavor of the B meson at the time of production [33]: the same–side tag, the soft–lepton tag and a jet–charge tag. Fig. 21 shows the true asymmetry

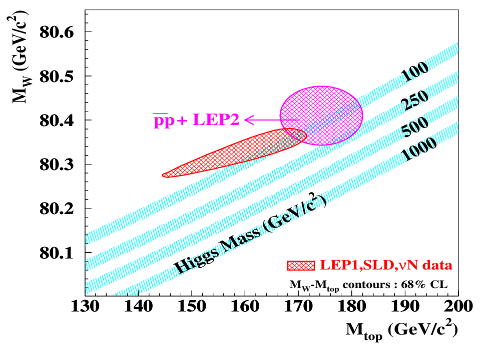

Figure 20. Current world averages for the direct W boson and top quark mass measurements from DØ, CDF and LEP experiments. The bands show SM predictions for the indicated Higgs masses [39].

(sin2β) as a function of lifetime for $B \to J/\psi K_S^0$ events. The non–SVX events, for which precision lifetime information is not available, are shown as a single point on the right. A maximum likelihood method is used to extract the result of $\sin 2\beta = 0.79 \pm 0.39(\mathrm{stat}) \pm 0.16(\mathrm{syst})$. This measurement is the best indication that CP symmetry is violated in the b quark system and is consistent with the Standard Model expectation of a large positive value of sin2β [34].

KTeV reports a new measurement of the direct CP violation parameter $Re(\epsilon'/\epsilon)$ using 23% of the data collected during the 1996–1997 fixed target run. It is well known that, in the neutral K meson system, the two strangeness states $(K^0, \overline{K}^0)$ mix to produce short and long lived kaons (K_S, K_L). In 1964, the observation of $K_L \to \pi\pi$ decays [40] revealed that CP symmetry is violated by the weak interaction. The dominant effect is an asymmetry in the $K^0 - \overline{K}^0$ mixing, parameterized by ϵ. Direct CP violation refers to the $K^0_{S,L} \to \pi^+\pi^-$ decays, in which a true CP eigenstate decays to a final state with opposite CP. The most sensitive searches for direct CP violation [41] measure

$$Re(\epsilon'/\epsilon) \approx \frac{1}{6}\left[\frac{\Gamma(K_L^0 \to \pi^+\pi^-)/\Gamma(K_S^0 \to \pi^+\pi^-)}{\Gamma(K_L^0 \to \pi^0\pi^0)/\Gamma(K_S^0 \to \pi^0\pi^0)} - 1\right].$$

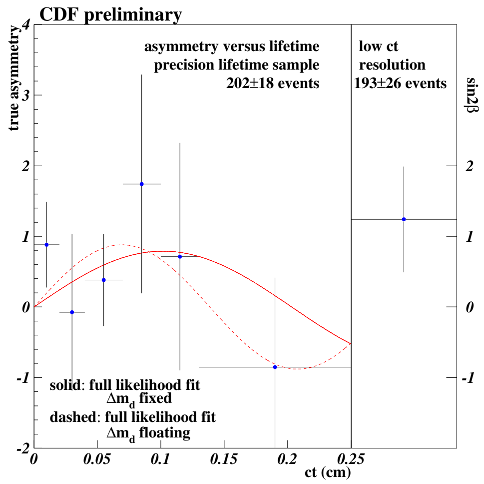

Figure 21. The true asymmetry (sin2β) as a function of lifetime for $B \to J/\Psi K_S^0$ events from CDF. The non–SVX events that lack precision lifetime information are shown as a single point on the right.

In this experiment, 800 GeV protons from the Tevatron are used to produce two K_L^0 beams; a regenerator in one of the beams (alternating once per minute) converts some K_L^0 to K_S^0 by coherent forward scattering. Kaon decays in the "vacuum beam" (K_L^0) and "regenerator beam" (mostly K_S^0) are collected simultaneously with the KTeV detector. $Re(\epsilon'/\epsilon)$ is extracted from the data using a fitting program which calculates decay distributions using full treatments of kaon production and regeneration. The measured value of $Re(\epsilon'/\epsilon) = (28.0 \pm 3.0(\mathrm{stat}) \pm 2.8(\mathrm{syst})) \times 10^{-4}$ firmly establishes the existence of CP violation in the decay process and rules out the "superweak" model [42]. Standard Model calculations of $Re(\epsilon'/\epsilon)$ depend sensitively on input parameters and the method of calculations [43]; it remains to be seen whether this large value of $Re(\epsilon'/\epsilon)$ can be accommodated or may be an indication of new physics beyond the Standard Model.

6. CONCLUSIONS

Although the Tevatron experiments have stopped taking data several years ago, the number of new results is overwhelming. The unprecedented precision in the experimental results that is being achieved is confronting theory with experiments at new limits. So far, QCD has held up to all the quantitative tests that were performed. We expect to see improvements in the calculations in the following years while the experiments prepare for a new period of data taking in which the Tevatron will continue to improve our understanding of nature.

Acknowledgements: I would like to thank my Tevatron colleagues who have provided me with the results included in this review, especially Andrew Brandt, Daniel Elvira, Ulrich Heintz, Rob Snihur and Mike Strauss from DØ, Alex Akopian, Mike Albrow, Frank Chlebana and Barry Wicklund from CDF, Marek Zielinski from E706, Donald Isenhower from E866, Peter Shawhan from KTeV, and Jeff Appel from E791. I would also like to thank the DIS99 organizers for an extremely interesting workshop.

REFERENCES

1. Jorge Morfin, "Near–and–Far Future DIS Experiments at Fermilab", this conference.
2. S. D. Ellis, Z. Kunszt, and D. E. Soper, Phys. Rev. Lett. **64** (1990) 2121.
3. F. Aversa, *et al.*, Phys. Rev. Lett. **65** (1990).
4. W. T. Giele, E. W. N. Glover, and D. A. Kosower, Phys. Rev. Lett. **73** (1994) 2019.
5. H. L. Lai *et al.*, Phys. Rev. D**55** (1997) 1280.
6. A. D. Martin *et al.*, Eur. Phys. J. **C4** (1998)463.
7. A. Akopian for the CDF Collaboration, WGIII, this conference.
8. The DØ Collaboration, Phys. Rev. Lett. **82** (1999) 2451.
9. D. Elvira for the DØ Collaboration, WGIII, this conference.
10. W.T. Giele, E.W.N. Glover and D.A. Kosower, Phys. Rev. Lett. **73** (1994) 2019.
11. The DØ Collaboration, Phys. Rev. Lett. **82** (1999) 2457.
12. F. Chlebana for the CDF Collaboration, WGIII, this conference.
13. H. Schellman for the DØ Collaboration, WGIII, this conference.
14. R. Snihur for the DØ Collaboration, WGIII, this conference.
15. G. Marchesini *et al.*, Comput. Phys. Commun. **67** (1992) 465.
16. K. Mauritz for the DØ Collaboration, WGII, this conference.
17. K. Borras for the CDF Collaboration, WGII, this conference.
18. L. Montanet *et al.* (Particle Data Group), Phys. Rev. **D54** (1996) 1.
19. R. Hamberg, W.L. van Neerven and T. Matsuura, Nucl. Phys. **B359** (1991) 343. W.L. van Neerven and E.B. Zijlstra, Nucl. Phys. **B382**(1992) 11.
20. J.L. Rosner, M.P. Worah, and T. Takeushi, Phys. Rev. **D49** (1994) 1363.
21. P. Arnold and R. Kauffman, Nucl. Phys. B**B349**(1991) 381.
22. C. Balasz and C. P. Yuan, Phys. Rev. **D56**(1997) 5558.
23. P.B. Arnold and M. H. Reno, Nucl. Phys. **B319** (1989) 37.
24. S. Kuhlmann for the CDF and DØ collaborations, WGIII, this conference.
25. W. Vogelsang and A. Vogt, Nucl. Phys. **B453** (1995) 334.
26. H.U. Bengtsson and T. Sjorstrand, Comput. Phys. Commun. **46** (1987) 43.
27. Michael Begel for the E706 Collaboration, WGI, this conference.
28. L. Apanasevich *et al.*, Phys. Rev. **D59** (1999) 74007.
29. J. F. Owens, Rev. Mod. Phys. **59** (1987) 465.
30. The DØ Collaboration, to be published in Phys. Rev. Lett. .
31. Donald Isenhower for the E866 Collaboration, WGI, this conference.
32. `http://www-cdf.fnal.gov/physics/new/bottom/cdf4855/cdf4855.html`.
33. M. Gronau *et al.*, Phys. Rev. **D47** (1994) 254. CDF Collaboration FERMILAB-PUB-99/019-E.
34. P. Paganini *et al.*, Phys. Scripta **58** (1998)

556. S. Mele CERN–EP–98–133, Aug. 1998, Submitted to Phys. Lett. **B**. A. Ali abd D. London, Nucl. Phys. Proc. Suppl. **54A** (1997) 297.

35. A. Sirlin, Phys. Rev. **D22** (1980) 971; W. Marciano and A. Sirlin, Phys. Rev. **D22** (1980) 2695; erratum-*ibid.* **31** (1985) 213.
36. S. Eidelmann and F. Jegerlehner, Z. Phys. **C67** (1995) 585.
37. `http://www-cdf.fnal.gov/physics/ewk/wmass_new.html`
38. `http://www-d0.fnal.gov/public/wz/wmass/wmass.html`
39. G. Degrassi, P. Gambino, and A. Sirlin, Phys. Lett. **B394**, (1997) 188.
40. J. H. Christenson *et al.*, Phys. Rev. Lett. **13** (1964) 138.
41. B. Winstein and L. Wolfenstein, Rev. Mod. Phys. **65** (1993) 1113.
42. L. Wolfenstein, Phys. Rev. Lett. **13** (1964) 562.
43. S. Bertolini, J. O. Eeg, and M. Fabbrichesi, hep-ph/9802405 (to appear in Rev. Mod. Phys.)